Hydroxylated 3-(pyridin-2-yl)coumarins as potential lipoxygenase inhibitors with relevant antioxidant activity

Sebastiano Masuri[1], Maria Grazia Cabiddu[1], Enzo Cadoni[1], Tiziana Pivetta[1]*

[1] Dipartimento di Scienze Chimiche e Geologiche, Università degli Studi di Cagliari, Cittadella Universitaria, 09042 Monserrato CA – Italy

Abstract

In the present study, 3-(pyridin-2-yl)coumarins with and without hydroxyl groups were prepared and their antioxidant and soybean lipoxygenase inhibitory activities were evaluated. Hydroxylated derivatives proved to possess potent lipoxygenase activities (IC_{50} under the μM range), with radical scavenging properties that are tuneable according to the number and position of the hydroxyl groups. The antioxidant properties and the way of enzymatic inhibition of the studied molecules were discussed based on calculated specific thermochemical descriptors and molecular docking.

The druglikeness of the synthesized molecules have been evaluated by merging theoretical calculations with experimental protonation constants, obtained from combined potentiometric and spectrophotometric titrations in aqueous solution.

Introduction

Coumarins comprise a large class of natural-based and synthetic compounds containing a 2*H*-chromen-2-one ring. Coumarins attract the attention of many scientists for their wide range of biological properties, such as antimicrobial, anticoagulant, antioxidant, anti-inflammatory and anticancer,[1–4] tuneable according to the nature and position of the substituents.

Hydroxyl ($^{\cdot}OH$), superoxide ($O_2^{-\cdot}$), hydroperoxide ($HOO^{\cdot}$), peroxides ($ROO^{\cdot}$), H_2O_2 and singlet oxygen ($^1O_2$) are Reactive Oxygen Species (ROS), commonly produced in biological systems as

natural by-products of cell metabolism, in concentrations finely controlled by a panel of endogenous antioxidant enzymes and small molecules.[5] However, under the influence of external factors, the concentration of ROS can increase dramatically, making the action of the ubiquitous detoxification system no more adequate. This imbalance, known as Oxidative Stress, leads to the damage of several intracellular components (DNA, lipids, proteins etc.) and is thought to be involved in various pathological conditions, that include cancers, inflammatory diseases, neurological disorders and ageing.[6]

Lipoxygenases constitute a class of non-heme, non-sulphur Iron dioxygenases that converts linoleic, arachidonic and other polyunsaturated fatty acids to yield hydroperoxides. Lipoxygenases exist in various isoforms and are particularly widespread in plants, animals and fungi.[7] Human lipoxygenases, 5-lipoxygenase (5-LOX) are involved in the arachidonic cascade, which is responsible of the production of leukotrienes,[8] that act as chemical mediators of several inflammatory and allergic phenomena (asthma, psoriasis and rheumatoid arthritis).[9,10] Increased levels of 5-LOX have also been observed in several types of tumours, in brain, colon and lungs, and several 5-LOX inhibitors have shown the ability of arresting the tumour cells proliferation, also inducing the apoptosis.[11]

Hydroxycoumarins have shown to possess antioxidant properties, thanks to their capability to go through radical processes, in a similar fashion to other potent antioxidant compounds, such as phenols and quinones.[12–17] In fact, the radicals obtained from hydroxycoumarins are structurally related to the phenoxide and semiquinone ones, with the unpaired electron that can be delocalized thanks to the π electron systems and/or the presence of electron-withdrawing functional groups, showing as a consequence, an interesting antioxidant activity.

In this work, the synthesis, the antioxidant ability (DPPH assay) and the evaluation of the inhibition mode towards soybean lipoxygenase of 3-(pyridin-2-yl)coumarin (**1-5**, **Scheme 1**) are discussed. Moreover, since protonation state and charge affect the absorption and the potential biological properties of the molecules,[18–23] the protonation constants of **1-5** were also determined. The calculation of specific thermochemical descriptors by quantomechanical calculation helped to explain

the antioxidant properties of the molecules, while molecular docking studies evidenced the possible way of enzymatic inhibition.

Experimental

Material and methods

Sodium chloride, sodium hydroxide, anhydrous ethanol, methanol, piperidine, lipoxygenase, sodium linoleate, 1,1-diphenyl-2-picrylhydrazyl free radical (DPP$^{\cdot}$), deuterated chloroform and tris (hydroxymethyl)aminomethane hydrochloride (TRIS) were purchased from Merck (Milan, Italy). Pyridine-2-acetonitrile, deuterated dimethyl sulfoxide, salicylic aldehyde and its derivatives were purchased from Alfa-Aesar. HCl Normex N/10 was purchased from Carlo Erba Reagents. The commercial reagents were used as received, without any further purification. Ultrapure water was obtained from MilliQ Millipore.

NMR measurements

^{1}H and ^{13}C NMR spectra were recorded on Varian UNITY INOVA 500 and Bruker Avance III HD 600 spectrometers at room temperature with tetramethylsilane (TMS) as internal standard in DMSO d_6. Chemical shifts, multiplicity and coupling constants were reported.

Mass spectrometry studies

Mass spectra were recorded using a triple quadrupole QqQ Varian 310-MS mass spectrometer using the atmospheric pressure ESI technique. Mass spectra were recorded by direct infusion of the sample solutions. The experimental conditions for positive mode were needle voltage 4500 V, shield 600 V, source temperature 100 °C, drying gas pressure 20 psi, nebulizing gas pressure 20 psi, detector voltage 1450 V, range 100–500 *m/z*.

Potentiometric and spectrophotometric titrations

Potentiometric titrations were carried out in a thermostatted vessel with a Mettler-Toledo Seven Compact pH/Ion-meter, equipped with a Mettler-Toledo InLab Micro Pro combined glass electrode

with an integrated temperature probe. Potentiometric titrations were performed at 25 °C in 0.1 M ionic strength (NaCl) under Ar atmosphere. The glass electrode was calibrated daily by titration of a known amount of HCl with carbonate-free NaOH standard solution prepared as previously reported.[24] Electrode standard potential (E^0), water ionic product (pK_w), electrode response and carbonate content of the titrant solution were checked with Gran's procedure using the GLEE software package.[25] The UV–Visible (UV–Vis) measurements were carried out with an Agilent Cary 60 spectrophotometer using a quartz cuvette with an optical path of 0.5 cm. Protonation constants of the studied compounds were determined by spectrophotometric and potentiometric titrations, at 25 °C in 0.1 M ionic strength buffer (NaCl). Solutions of ligands were prepared daily by dissolving the proper amount of the compound in DMSO (concentrations ~13 mM) prior to the proper dilutions in NaCl 0.1 M (final DMSO content ≤ 1 % V/V). Operative concentrations of the ligands ranged from 1.24×10^{-4} M to 1.30×10^{-4} M according to their absorptivity. Four HCl equivalents for **1** and five HCl equivalents for the other ligands were added before the titration. A known aliquot of these solutions was titrated with NaOH standard solution. Both potentiometric and spectrophotometric data were simultaneously analysed using the Hyperquad 2006 suite.[26] Speciation diagrams were obtained using Hyss 2009 software.[27]

Determination of the reducing activity of the stable radical 1,1-diphenyl-picrylhydrazyl (DPP·)

Each test compound was dissolved in DMSO at 1.0 mM concentration, and then a 1:10 dilution was performed with absolute ethanol. DPP· solution (0.1 mM, absolute ethanol) was prepared freshly, stored in the dark and used in a few hours. The test solution (1500 µL) was added to an equal volume of DPP· inside the cuvette and the absorbance in the 300–650 nm range was recorded at room temperature for 70 minutes. The final concentrations for both DPP· and the tested compounds were 50 µM. The absorbance at 517 nm was evaluated to examine the time-dependence of the radical

scavenging activity (RA).[28] The RA of each compound was expressed as the percentage inhibition of the absorbance of the initial DPP· solution (RA%).

Soybean lipoxygenase inhibition study in vitro

Stock solutions of compounds **1-5** were prepared by dissolving them in DMSO at ≈ 0.1 mM concentration, and then a proper dilution was performed with TRIS buffer at pH 7.4. Sodium linoleate (0.0013 g, V 10.0 mL, 4.30 10^{-4} M) and soybean lipoxygenase (0.0013 g, V 10.0 mL, 1.24 10^{-6} M) were dissolved in TRIS buffer at pH 7.4 and diluted with TRIS buffer at pH 7.4. Solutions of sodium linoleate, soybean lipoxygenase and **1-5** were prepared daily and kept in the dark at 25 °C. The conversion of sodium linoleate to 13-hydroperoxylinoleic acid was monitored by recording the absorbance at 243 nm, and not at 234 nm (absorption maximum) was chosen since at 234 nm the contribution of **1-5** absorbances were not negligible.

DFT calculations

DFT calculations were performed using the release 4.2.0 of the ORCA software package.[29] Input files for DFT calculations were prepared using Avogadro 1.2.0.[30] Geometry optimizations were performed using the hybrid PBE0 functional[31] and def-2 TZVP basis set.[32] IR frequency calculations were carried out to verify the nature of the minima of each optimization by evaluating the absence of calculated negative frequencies. DFT calculations were performed both at gas phase and in presence of the solvent (ethanol, water). Solvent effects were considered using the conductor-like polarizable continuum model (CPCM).[33] Molecular orbital shapes and energies, electrostatic potential surfaces were investigated using Chemcraft v1.8.[34] Atomic charges at Natural Population Analysis (NPA) level were calculated using the JANPA software package.[35]

Several thermochemical parameters were calculated, starting from the appropriate enthalpy values, to give more insights about the preferred pathways chosen by the studied compounds to exert their antioxidant properties. The following mechanisms, commonly adopted by antioxidant phenolics, were considered:[16,36–39]

1. Hydrogen Atom Transfer (**HAT**), where a radical hydrogen is directly abstracted from the phenolic antioxidant (**R1**). The Bond Dissociation Enthalpy (**BDE, eq.1**) quantitatively describes this reaction path.

$ArOH \rightarrow ArO^{\cdot} + H^{\cdot}$ $(\boldsymbol{R1})$ $\qquad$ $\boldsymbol{BDE} = H(ArO^{\cdot}) + H(H^{\cdot}) - H(ArOH)$ $(\boldsymbol{eq.1})$

2. Single Electron Transfer Proton Transfer (**SETPT**), where the extraction of an electron from the antioxidant (**R2a**) is followed by proton removal from the subsequent radical cation (**R2b**). Ionization Potential (**IP, eq.2a**) and Proton Dissociation Enthalpy (**PDE, eq.2b**) are commonly exploited to describe the two steps, respectively. The thermochemical parameter **SETPT** (**eq.2**) considers the process in its entirety.

$ArOH \rightarrow ArOH^{+\cdot} + e^{-}$ $(\boldsymbol{R2a})$ $\qquad$ $\boldsymbol{IP} = H(ArOH^{+\cdot}) + H(e^{-}) - H(ArOH)$ $(\boldsymbol{eq.2a})$

$ArOH^{+\cdot} \rightarrow ArO^{\cdot} + H^{+}$ $(\boldsymbol{R2b})$ $\qquad$ $\boldsymbol{PDE} = H(ArO^{\cdot}) + H(H^{+}) - H(ArOH^{+\cdot})$ $(\boldsymbol{eq.2b})$

$\boldsymbol{SETPT} = \boldsymbol{IP} + \boldsymbol{PDE}$ $(\boldsymbol{eq.2})$

3. Sequential Proton Loss Electron Transfer (**SPLET**), where the phenolic antioxidant is firstly deprotonated (**R3a**) then converted in its neutral radical by single electron transfer (**R3b**). The first step is described by the Proton Affinity (**PA, eq.3a**), while the second one is quantitatively defined by the Electron Transfer Enthalpy (**ETE, eq.3b**). The thermochemical parameter **SPLET** (**eq.3**) contemplates the process in its entirety.

$ArOH \rightarrow ArO^{-} + H^{+}$ $(\boldsymbol{R3a})$ $\qquad$ $\boldsymbol{PA} = H(ArO^{-}) + H(H^{+}) - H(ArOH)$ $(\boldsymbol{eq.3a})$

$ArO^{-} \rightarrow ArO^{\cdot} + e^{-}$ $(\boldsymbol{R3b})$ $\qquad$ $\boldsymbol{ETE} = H(ArO^{\cdot}) + H(e^{-}) - H(ArO^{-})$ $(\boldsymbol{eq.3a})$

$\boldsymbol{SPLET} = \boldsymbol{PA} + \boldsymbol{ETE}$ $(\boldsymbol{eq.3})$

The enthalpy for the hydrogen atom was calculated both at gas phase and in presence of solvents using the same computational setup. The enthalpies in gas phase for proton and electron were taken from the literature as 1.481 and 0.752 kcal/mol respectively.[40,41] The enthalpies for proton and electron in solvent were calculated by assuming the solvation of a proton or an electron with a molecule of solvent using CPCM, as previously reported.[37,41] Both the chemical formalisms and the equations used for the calculation of these enthalpies are reported down below.

$$H^{+}_{(gas)} + H_2O_{(aq)} \rightarrow H_3O^{+}_{(aq)}$$

$$\boldsymbol{H\left[H^{+}_{(aq)}\right] = H\left[H_3O^{+}_{(aq)}\right] - H\left[H_2O_{(aq)}\right] - H\left[H^{+}_{(gas)}\right]}$$

$$H_2O_{(aq)} + e^{-}_{(gas)} \rightarrow H_2O^{-\cdot}_{(aq)}$$

$$\boldsymbol{H\left[e^{-}_{(aq)}\right] = H\left[H_2O^{-\cdot}_{(aq)}\right] - H\left[H_2O_{(aq)}\right] - H\left[e^{-}_{(gas)}\right]}$$

$$H^{+}_{(gas)} + CH_3CH_2OH_{(solv)} \rightarrow CH_3CH_2OH_2^{+}{}_{(solv)}$$

$$\boldsymbol{H\left[H^{+}_{(solv)}\right] = H\left[CH_3CH_2OH_2^{+}{}_{(solv)}\right] - H\left[CH_3CH_2OH_{(solv)}\right] - H\left[H^{+}_{(gas)}\right]}$$

$$CH_3CH_2OH_{(solv)} + e^{-}_{(gas)} \rightarrow CH_3CH_2OH^{-\cdot}_{(solv)}$$

$$\boldsymbol{H\left[e^{-}_{(solv)}\right] = H\left[CH_3CH_2OH^{-\cdot}_{(solv)}\right] - H\left[CH_3CH_2OH_{(solv)}\right] - H\left[e^{-}_{(gas)}\right]}$$

Molecular descriptors

Molecular descriptors, such as miLogP (calculated logarithm of the partition coefficient), TPSA (Topological Polar Surface Area), number of hydrogen bond donors and acceptors, rotatable bonds, molecular weight, molecular volume and Number of violation of the Lipinski's Rule of five were calculated using the Molinspiration property software (v2018.10).[42]

Molecular docking

Molecular docking calculations were performed using Autodock Vina software.[43] DFT optimized structure of the ligands were exported as PDB files. The X-ray structure of soybean lipoxygenase LOX-1 (PDB:3PZW) was chosen as the receptor. Prior to docking, both ligands and receptor were processed using MG Labs Autodock Tools.[44] In the receptor structure, water molecules were removed while polar hydrogens and Gasteiger charges were added. The atomic charge for the Fe2840 cofactor was manually adjusted in the generated pdbqt file. For all the ligands, polar hydrogens and Gasteiger charges were added, no rotational constraints were applied. All the tested compounds were docked using a grid cube of 30 × 30 × 30 points centred at Iron cofactor coordinates (x = 24.527, y = 44.349, z = 10.587) with a spacing of 1.0 Å and an exhaustiveness value of 100. Molecular interactions and docked poses were evaluated using Biovia Discovery Studio Viewer v19.[45]

Synthesis

General procedure for the preparation of chromene-2-one derivatives.[46,47] Salicylaldehyde derivatives (0.0072 mol) and pyridine-2-acetonitrile (0.76 mL, 0.0072 mol) were dissolved in 14 mL of anhydrous ethanol, and piperidine (0.26 mL) was added dropwise in an ice bath. The mixture was stirred for 20 h at room temperature, treated with HCl (23 mL, 3.5 %) and refluxed for 10 h to hydrolyse the iminocoumarin. For compounds **1**, **2**, **3** and **5** the resulting acidic solution was neutralized with aqueous ammonia until pH 7, affording a precipitate that was recovered by filtration. In the case of **4**, the formed solid product was immediately recovered. The crude products were recrystallized from methanol to yield the desired products. Compound **1** was previously prepared and characterized.[46,47]

2 (7-Hydroxy-3-(pyridin-2-yl)-2*H*-chromen-2-one): Yield was 65%. Experimental results are in accordance with those reported in literature.[48] ^{1}H NMR (500 MHz, DMSO d_6, δ, ppm, **Fig. S1**): 8.79 (s, 1H), 8.65 (dt, J = 4.7, 1.4 Hz, 1H), 8.23 (dt, J = 8.1, 1.2 Hz, 1H), 7.85 (td, J = 7.8, 1.9 Hz, 1H), 7.74 (d, J = 8.5 Hz, 1H), 7.36 (ddd, J = 7.5, 4.7, 1.1 Hz, 1H), 6.83 (dd, J = 8.5, 2.3 Hz, 1H), 6.76 (d, J = 2.1 Hz, 1H). ESI-MS (calcd, found, *m/z*): 240.1, 240.1 $[M+H]^+$ (**Fig. S7A**).

3 (5,7-dihydroxy-3-(pyridin-2-yl)-2*H*-chromen-2-one): Yield was 50 %. ^{1}H NMR (600 MHz, DMSO d_6, δ, ppm, **Fig. S2**): 8.97 (s, 1H), 8.65 (dd, *J* = 4.9, 1.8 Hz, 1H), 8.28 (d, *J* = 8.1 Hz, 1H), 7.85 (td, *J* = 7.8, 1.9 Hz, 1H), 7.34 (dd, *J* = 7.5, 4.7 Hz, 1H), 6.33 (d, *J* = 2.1 Hz, 1H), 6.26 (d, *J* = 2.1 Hz, 1H). ^{13}C NMR (151 MHz, DMSO d_6, δ, ppm, **Fig. S3**): 163.64, 160.54, 157.53, 156.83, 152.13, 149.76, 138.58, 137.12, 123.07, 122.95, 117.96, 102.92, 98.51, 94.17. ESI-MS (calcd, found, *m/z*): 256.0, 256.1 $[M+H]^+$ (**Fig. S7B**).

4 (6,7-dihydroxy-3-(pyridin-2-yl)-2*H*-chromen-2-one): Yield was 3 5%. ^{1}H NMR (600 MHz, DMSO d_6, δ, ppm, **Fig. S4**): 8.74 (s, 1H), 8.70 (dd, *J* = 5.4, 1.7 Hz, 1H), 8.31 (d, 8.2 Hz, 1H), 8.18 (t, *J* = 8.0 Hz, 1H), 7.60 (t, *J* = 6.5 Hz, 1H), 7.12 (s, 1H), 6.82 (s, 1H). ^{13}C NMR (151 MHz, DMSO d_6, δ, ppm,

Fig. S5) δ 160.24, 153.47, 149.95, 149.83, 145.98, 145.93, 145.60, 144.22, 141.8, 124.94, 124.62, 113.57, 111.42, 102.84. ESI-MS (calcd, found, *m/z*): 256.0, 256.1 $[M+H]^+$ (**Fig. S7C**).

5 (7,8-dihydroxy-3-(pyridin-2-yl)-2*H*-chromen-2-one): Yield was 52 %. Experimental results are in accordance with those reported in literature[48]. ^{1}H NMR (600 MHz, DMSO d_6, δ, ppm, **Fig. S6**): 8.77 (s,1H), 8.67 (dt, *J* = 4.6, 1.5 Hz, 1H), 8.28 (dd, *J* = 8.1, 1.2 Hz, 1H), 7.88 (td, *J* = 7.8, 1.9 Hz, 1H), 7.38 (ddd, *J* = 7.6, 4.8, 1.1 Hz, 1H), 7.25 (d, *J* = 8.4 Hz, 1H), 6.87 (d, *J* = 8.4 Hz, 1H). ESI-MS (calcd, found, *m/z*): 256.0, 256.1 $[M+H]^+$ (**Fig. S7D**).

Results and discussion

Chemistry

3-(Pyridin-2-yl)coumarin (**1**) and its hydroxylated derivatives (**2-5**) were prepared starting from the appropriate hydroxylated benzaldehyde and pyridine-2-acetonitrile via Knovenagel Condensation and subsequent acidic hydrolysis. This step was required to convert the iminocoumarins obtained *in-situ* in the desired products.

The synthetic pathway and the acronyms of the studied compounds are reported in **Scheme 1**. The novel derivatives **3** and **4** were obtained with 50 % and 35 % yields, respectively. Structures and purity of the studied compounds were assessed via ^{1}H-NMR (**Fig. S1, S2, S4, S6**) and ESI-MS (**Fig. S7**). ^{13}C-NMR analyses were additionally performed for **3** and **4** in order to provide a complete characterization for these novel compounds (**Fig. S3, S5**).

The studied compounds have been selected following specific criteria. Considering that natural hydroxycoumarins, such as Umbelliferone (7-hydroxycoumarin), Aesculetin (6,7-dihydroxycoumarin) and Daphnetin (7,8-dihydroxycoumarin), have shown both antioxidant and lipoxygenase inhibitory activities,[49–52] we decided to extend these substitution patterns to the scaffold of **1**. In particular, we firstly introduced a hydroxyl group in the 7th position (**2**), then we added an additional –OH in the 5th, 6th and 8th position (compounds **3**,**4** and **5** respectively). The heteroaryl

moiety in the 3rd position has been introduced with the aim of enhancing the electronic delocalization of the related phenoxide radicals and anions. In addition, the presence of a pyridyl nitrogen could be useful in improving water solubility (as hydrogen bond acceptor) and could be involved (in conjunction with the carbonyl oxygen) in the chelation of Iron (III) metal cofactor of lipoxygenases.

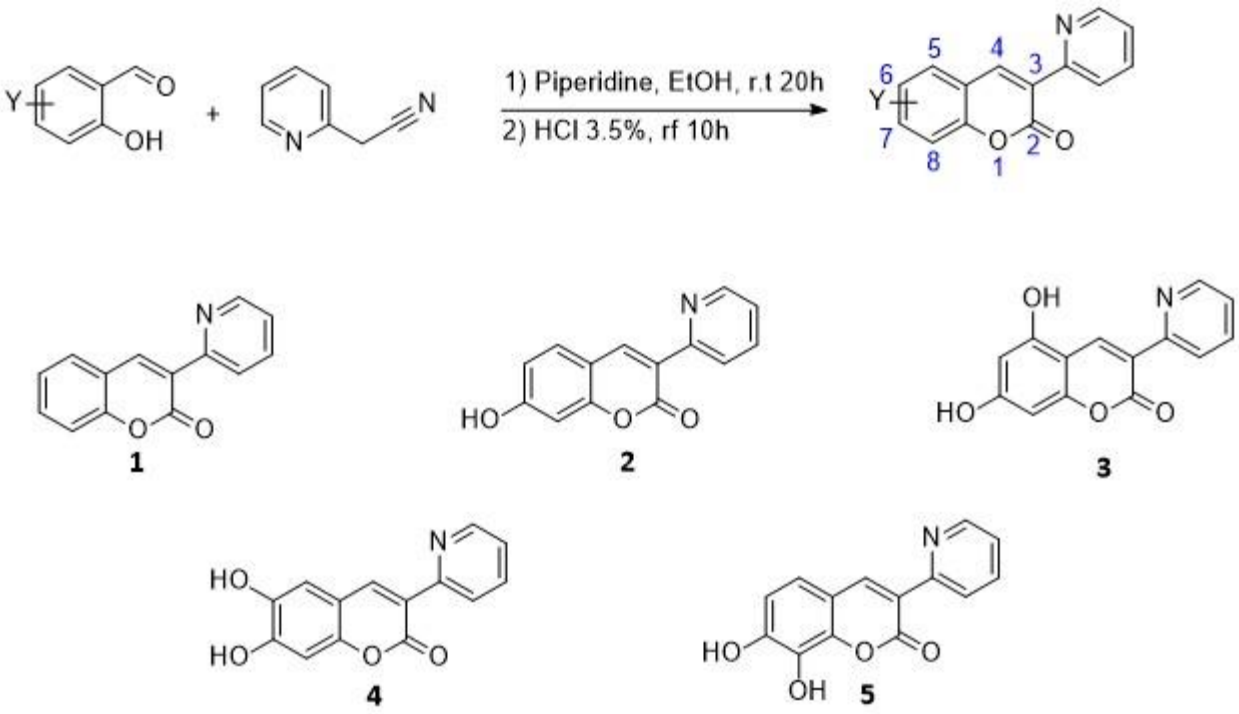

Scheme 1: Reaction Scheme and structures of the synthesized compounds.

Solution equilibria studies

The protonation constants of the studied compounds were determined by spectrophotometric and potentiometric titrations carried out simultaneously. Elaboration of the titration data was performed in the pH range 3 – 11 for ligands **2-5**. In contrast, for compound **1** the presence of an additional change in the spectral shape at pH > 10 (**Fig. S8**) made the results obtained from data elaboration in the same pH range unreliable. This behaviour in highly alkaline medium is attributable to the hydrolysis of the 2*H*-pyran-2-one moiety, as previously observed for similar systems.[53] For this reason, experimental data at pH > 10 were excluded from protonation constants determination of **1**, allowing to obtain more consistent results.

Selected spectra recorded during the titrations of the studied compounds are shown in **Fig. 1,** while the spectral variations observed for each ligand during the titrations are detailed in the Supporting section (**Fig. S9-S13**).

From the eigenvalue analysis of the spectrophotometric data, the number of linearly independent absorbing species as the significant eigenvalues, were found. In particular, three species were found for **1**, i.e. $\mathbf{H_2L^{2+}}$, $\mathbf{HL^{+}}$ and **L**, four species for **2**, i.e. $\mathbf{H_3L^{2+}}$, $\mathbf{H_2L^{+}}$, **HL**, and $\mathbf{L^{-}}$, and five species for **3-5**, i.e. $\mathbf{H_4L^{2+}}$, $\mathbf{H_3L^{+}}$, $\mathbf{H_2L}$, $\mathbf{HL^{-}}$, $\mathbf{L^{2-}}$. Potentiometric and spectrophotometric data were simultaneously fitted to obtain the cumulative formation constants (β) expressed as logarithms, the related pK values were calculated (**Table 1**). Absorptivity values taken at maximum wavelengths for all the absorbing species are summarized in **Table 2.** Calculated pure spectra are reported in **Fig. S14.**

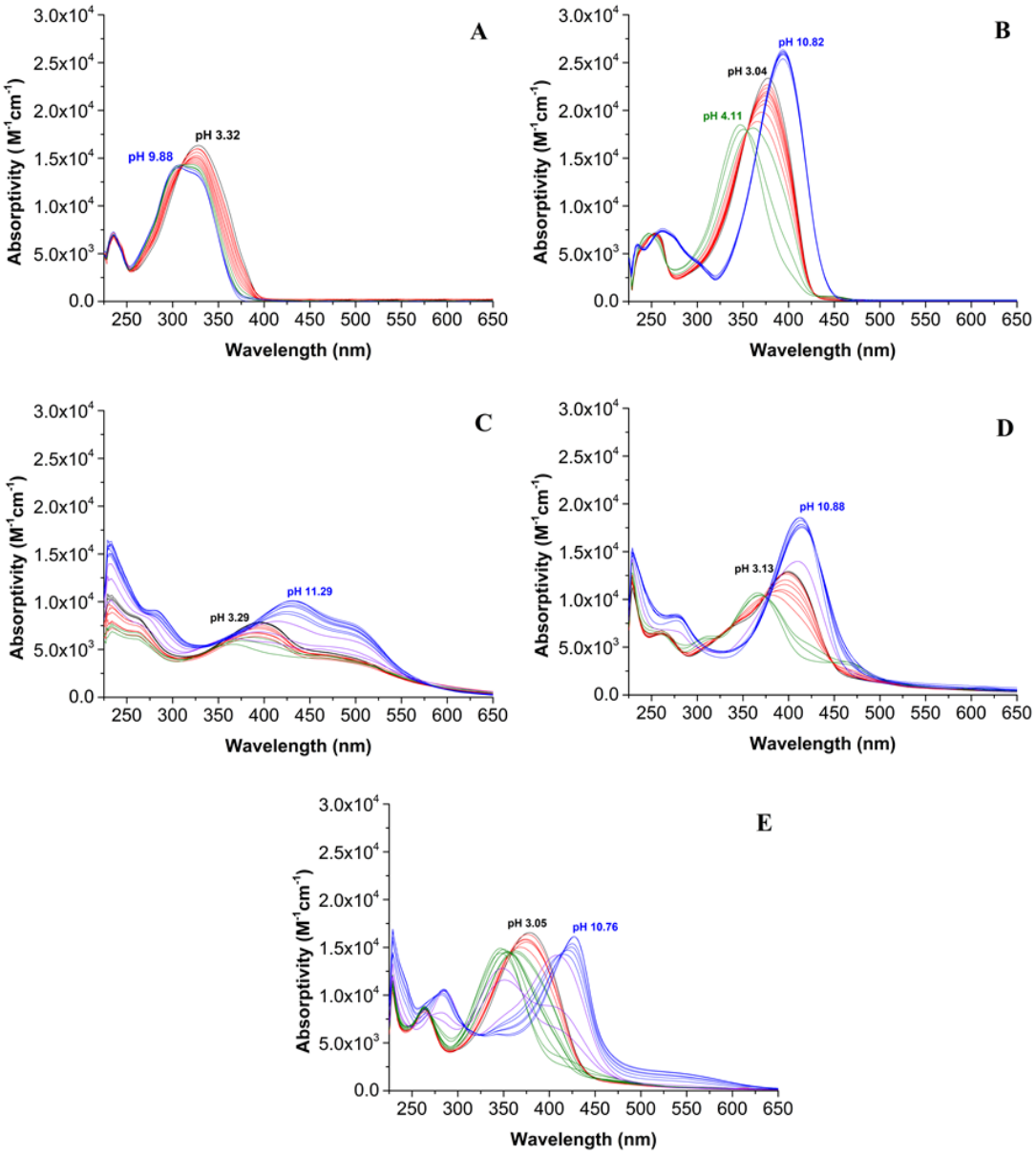

Fig. 1. Selected spectra, reported as absorptivity, collected during the potentiometric and spectrophotometric titrations of **1 - 5** (**A - E**)**,** *t* 25°C**,** NaCl 0.1 M.

Table 1. Protonation constants of **1-5** (*t* 25°C, NaCl 0.1 M). The standard deviation to the last significant figure is reported in parentheses.

COMPOUND	Equilibrium	Logβ	pK
1	$L + H^+ \rightleftharpoons HL^+$	4.12 (3)	4.12
	$L + 2H^+ \rightleftharpoons H_2L^{2+}$	7.77 (5)	3.65
2	$L^- + H^+ \rightleftharpoons HL$	6.39 (9)	6.39
	$L^- + 2H^+ \rightleftharpoons H_2L^+$	10.93 (9)	4.54

	$L^- + 3H^+ \rightleftharpoons H_3L^{2+}$	14.94 (5)	4.01
3	$L^{2-} + H^+ \rightleftharpoons HL^-$	9.43 (3)	9.43
	$L^{2-} + 2H^+ \rightleftharpoons H_2L$	15.28 (5)	5.85
	$L^{2-} + 3H^+ \rightleftharpoons H_3L^+$	20.0 (1)	4.72
	$L^{2-} + 4H^+ \rightleftharpoons H_4L^{2+}$	23.5 (1)	3.50
4	$L^{2-} + H^+ \rightleftharpoons HL^-$	9.82 (5)	9.82
	$L^{2-} + 2H^+ \rightleftharpoons H_2L$	16.19 (7)	6.37
	$L^{2-} + 3H^+ \rightleftharpoons H_3L^+$	20.4 (1)	4.21
	$L^{2-} + 4H^+ \rightleftharpoons H_4L^{2+}$	24.7 (1)	3.45
5	$L^{2-} + H^+ \rightleftharpoons HL^-$	9.76 (6)	9.76
	$L^{2-} + 2H^+ \rightleftharpoons H_2L$	15.94 (5)	6.18
	$L^{2-} + 3H^+ \rightleftharpoons H_3L^+$	20.2 (1)	4.26
	$L^{2-} + 4H^+ \rightleftharpoons H_4L^{2+}$	23.4 (1)	3.20

Table 2. Absorptivity values of the variously protonated species of **1-5** (*t* 25°C, NaCl 0.1 M).

COMPOUND	Species	λ_{max} (nm)	ε ($\times 10^4$ $M^{-1}cm^{-1}$)
1	L	310; 323 (sh)	1.42; 1.36
	HL^+	309; 323 (sh)	1.46; 1.43
	H_2L^{2+}	343	1.95
2	L^-	397	2.62
	HL	351	1.91
	H_2L^+	382	2.39
	H_3L^{2+}	379	2.30
3	L^{2-}	431; 494 (sh)	1.04; 0.78
	HL^-	362; 482 (sh)	0.55; 0.31
	H_2L	402; 487 (sh)	0.71; 0.47
	H_3L^+	393; 483 (sh)	0.64; 0.32
	H_4L^{2+}	401; 490 (sh)	1.09; 0.69
4	L^{2-}	415	1.98
	HL^-	368	1.11
	H_2L	405	1.39
	H_3L^+	376	1.18
	H_4L^{2+}	405	1.47
5	L^{2-}	425	1.90
	HL^-	348	1.67
	H_2L	352	1.40
	H_3L^+	372	1.61
	H_4L^{2+}	390	2.48

Molecular properties

Several molecular descriptors were calculated, as reported in **Table 3**. All the compounds here reported adhere to the Lipinski's rule of five, which states that poor absorption or permeation is more likely observed when there are more than 5 H-bond donors, 10 H-bond acceptors, the molecular weight (MW) is greater than 500 Dalton and the calculated LogP value is greater than 5.[54] The calculated miLogP range from 1.60 (for compound **4**) to 2.59 (for compound **1**), suggesting an acceptable compromise between lipophilicity (for membrane permeability) and hydrophilicity (for oral administration).

Table 3. Calculated molecular descriptors for the studied compounds.

	1	**2**	**3**	**4**	**5**
miLogP[a]	2.59	2.09	1.8	1.6	1.83
TPSA (Å^2)[b]	43.10	63.33	83.56	83.56	83.56
n-atoms[c]	17	18	19	19	19
MW (Da)	223.23	239.23	255.23	255.23	255.23
n-ON[d]	3	4	5	5	5
n-OHNH[e]	0	1	2	2	2
n-violations[f]	0	0	0	0	0
n-rotb[g]	1	1	1	1	1
volume (Å^3)[h]	195.84	203.86	211.87	211.87	211.87

[a] Calculated Logarithm of the partition coefficient between n-octanol and water (milogP); [b] topological polar surface area (TPSA); [c] number of atoms in the molecule (n-atoms); [d] number of hydrogen bond acceptors (n-ON); [e] number of hydrogen bond donors (n-OHNH); [f] number of violations of the Lipinski's rule of five; [g] number of rotatable bonds (n-rotb); [h] molecular volume**.**

The ability of a molecule to cross cellular membranes and Blood Brain Barrier (BBB) could also be preliminary evaluated by TPSA values,[55] which are correlated to the ability of a compound to form hydrogen bonds. For **1-5**, TPSA values range from 43.10 Å^2, for **1**, to 83.56 Å^2, for **3-5**. These values are far below the upper limit of 140 Å^2, thus supporting a good oral bioavailability. Moreover, for **2-5** the TPSA values, higher than 60 Å^2, suggest a BBB crossing ability from moderate to modest.[56]

As shown by solution equilibria experiments, the studied molecules exist in different protonation states according to the medium pH and, as a consequence, can exert different biological activity.[18,57] From the distribution diagrams obtained from the experimental pKs (**Fig. 2**) some consideration regarding the species potentially present in blood plasma and different compartments of the gastrointestinal (GI) tract could be made. In the blood plasma (pH 7.4), only **1** would be in neutral state (due to the absence of –OH groups), while the other compounds would be mainly present in their monoanionic form, i.e. $\mathbf{L}^-$ for **2**, and $\mathbf{HL}^-$ for **3-5**.

In the GI tract the situation appears more complicated since pH varies among the different regions, and also regional pH values fluctuate between and within individuals according to factors like presence of food, GI/systemic diseases, age, circadian rhythms, and concomitant drug administration.[58] In the stomach, pH of healthy young Caucasians lies below 3 for 90% of fasted state, while it could increase till 7 at fed state, thanks to the buffering effect observed after food ingestion. In the regions of intestine, pH varies in the range 4.9-7.4 at fasted state and between 5.2 and 7.5 at fed state.[59] By combining these average values with the data available, it is possible to make some hypothesis about the region where these molecules are more likely to be absorbed via passive diffusion mechanism. All the studied compounds appear to be more likely absorbed in the intestine, in particular at the beginning of duodenum (pH 4.9 at fasted state, 5.1 at fed state), since these molecules are predominantly in neutral state at these pH values. The same molecules could be absorbed in the stomach at fed state too, especially **1** thanks to the absence of hydroxyl groups. This information doesn't allow to exclude that **1-5** could cross the cell membranes in their monoanionic forms using other mechanisms. Additional pharmacokinetic studies would be required for this purpose but are outside the scope of this work.

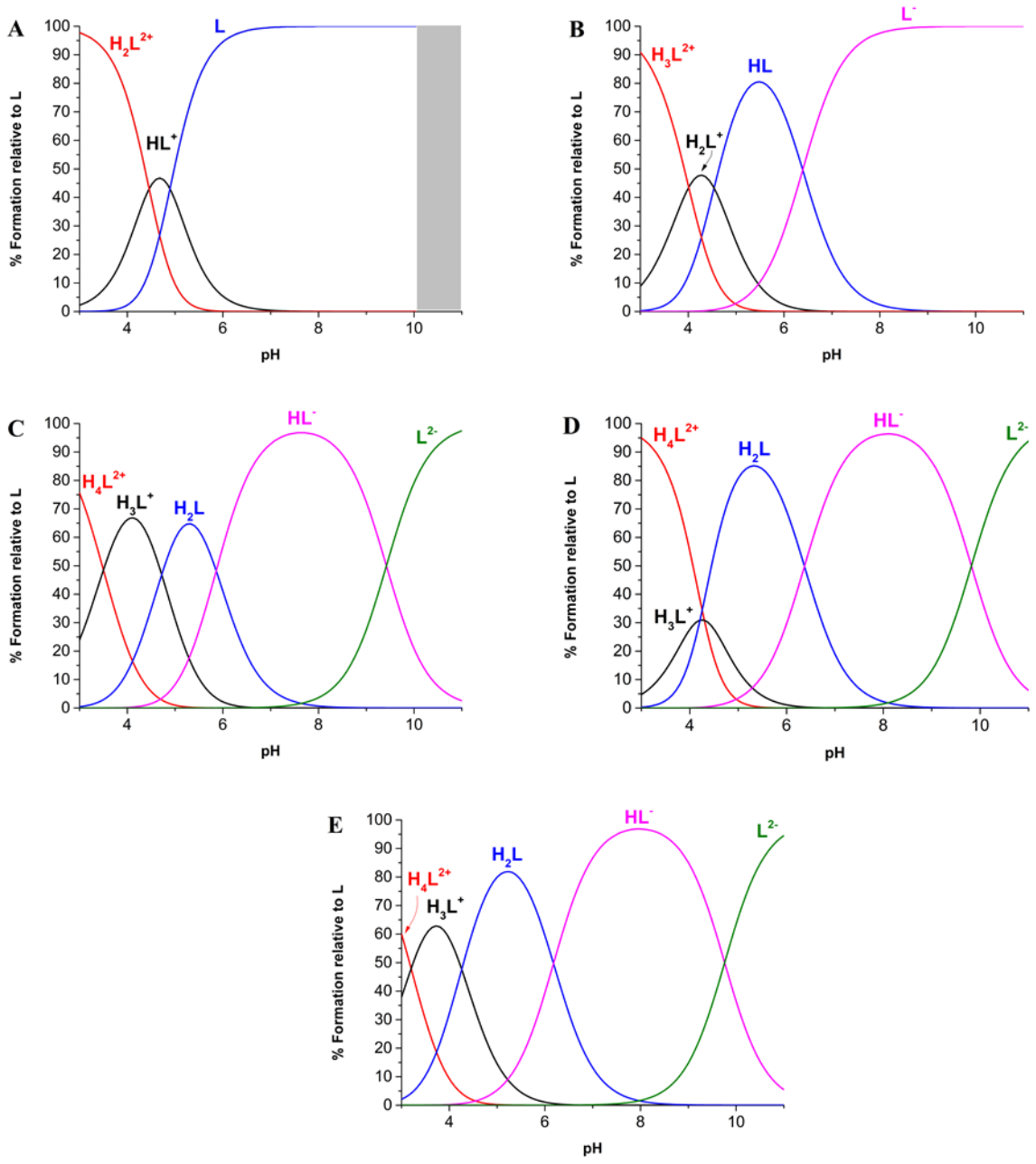

Fig. 2. pH distribution curves for **1**-**5** (**A**-**E**), **1** 1.26×10^{-4} M, **2** 1.24×10^{-4} M, **3** 1.30×10^{-4} M, **4** 1.25×10^{-4} M, **5** 1.25×10^{-4} M, *t* 25°C**,** NaCl 0.1 M

Antioxidant assays

Considering the involvement or ROS in the pathogenesis of several inflammatory diseases and neoplasms,[60] and the radical scavenging properties exerted by different Non-Steroidal Anti-Inflammatory Drugs (NSAIDs),[61,62] the antioxidant activity of **1**-**5** were evaluated by DPPH assay.

This test, commonly employed to evaluate the antioxidant activity of both synthetic and natural molecules, is based on the ability of the stable radical 1,1-diphenyl-picrylhydrazyl (DPP·) to accept a H· from the tested compound to be converted into the diamagnetic form (DPPH). The radical DPP· shows in absolute ethanol a deep violet colour (λ_{max} = 517 nm), while the diamagnetic DPPH is pale yellow coloured in the same solvent. The decrease in absorbance at 517 nm due to the radical hydrogen transfer can be followed through time and allows to compare the radical scavenging capacity of different compounds. Results for **1-5** are summarized in **Fig. 3A** and the variation of absorbance (as %) observed during time is shown in **Fig. S15**. Compound **1** possess negligible DPPH antioxidant activity, lower than 1 % at 20' or 60'. Comparing **1** with the other molecules, we can deduce that the insertion of a hydroxyl group in the 7th position of the 2*H*-cromen-2-one backbone, **2**, determines a modest increase in terms of RA% while the insertion of a second -OH, **3-5**, causes a significant increment, in particular when the two -OH groups are in ortho position, like in **4** and **5**. This trend is in agreement with the results reported for compounds having a catecholic moiety in their backbone.[12,63–65].

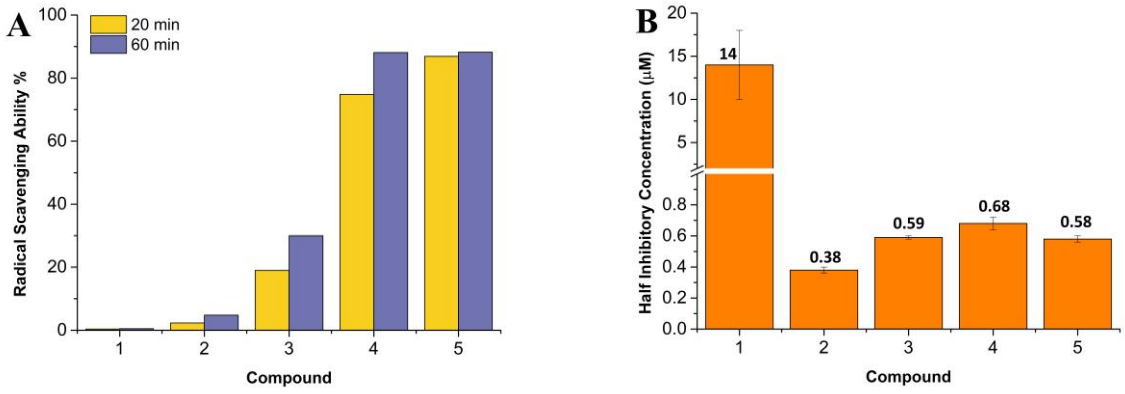

Fig. 3. (**A**) Radical Scavenging Activity (as %) of **1-5** on radical 1,1-diphenyl-picrylhydrazyl (DPP·); (**B**) Half Inhibitory Concentration of **1-5** towards Soybean Lipoxygenase.

Inhibition of Soybean Lipoxygenase in vitro

Soybean Lipoxygenase inhibition[66] studies were performed by keeping constants the concentrations of both enzyme and linoleic acid, while varying the concentrations of **1-5**. The increase in absorbance

at 243 nm due to the conversion of linoleic acid to 13-hydroperoxylinoleic acid was followed with time (**Fig. S16**) observing that: *i*) in absence of inhibitors the conversion to 13-hydroperoxylinoleic acid by Soybean Lipoxygenase is completed in approx. 60-70 minutes; *ii*) in the presence of **1**-**5** the conversion was never quantitative.

The Inhibition Percentage (IP%) reported as a function of the concentration of the tested inhibitor (**Fig. S17**) shows a trend time dependent, preventing an immediate calculation of the inhibitory concentration required to inhibit the 50% of the enzyme (IC_{50}). After 80' the observed trend become invariant, IP% was then mediated in the time interval 80-120' leading to the calculation of the IC_{50}, that resulted to be < 1 μM for all the molecules except **1** (14 ± 4 μM), varying in the order **2** > **5** > **3** > **4** >> **1**. These results, reported in **Fig. 3B,** show how the presence of one or two hydroxyl groups increases the inhibition ability of the molecules, however the less effect shown by the second -OH group could be explained in terms of augmented steric hindrance.

DFT calculations

Structural and electronic properties

DFT-optimized geometries for **1**-**5** in the gas phase are reported in **Fig. 4**. As can be seen, the pyridine moiety adopts a distorted antiperiplanar conformation in relation to the coumarin moiety. This feature is consistent with the crystal structure of **1**,[67] whose structural parameters (bond lengths, angles, dihedrals) are well reproduced by the DFT-optimized structure of the same compound (**Table S1**). Selected bond lengths, angles and dihedrals calculated for **2**-**5** are reported in **Table S2**-**S5**.

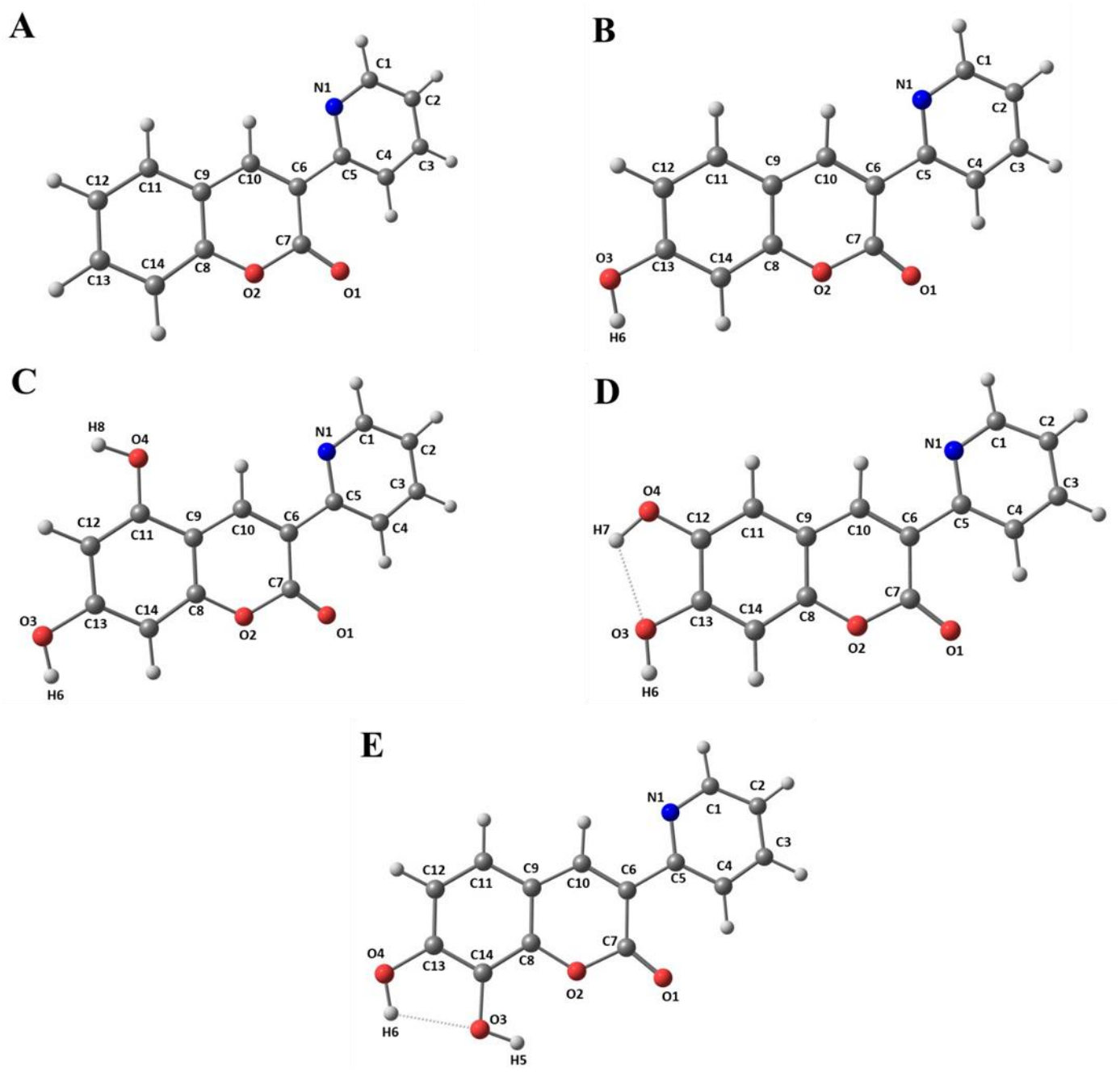

Fig. 4. Molecular drawings and atom labelling scheme for **1-5** (**A-E**) at the DFT-optimized geometries (gas phase).

Molecular Electrostatic Potential (MEP) surfaces help to visualize potential regions of different polarity to predict the reactivity with nucleophilic or electrophilic reactants and the presence of hydrogen bonding interactions. For compounds **2-5** the electropositive regions are localised on the hydrogen atoms of the -OH groups, while for **1** on the aromatic hydrogens of the 2-*H*-cromen-2-one

moiety; the most electronegative regions are detected in proximity of the heteroatoms (oxygens in particular), as shown in **Fig. S18**. These results are in accordance with the atomic charges, computed at both Mulliken and NPA level, reported in **Table S6-S10**.

A broad distribution of the frontier Molecular Orbitals (MOs) (**Fig. S19**) was observed in the 3-(pyridine-2-yl)coumarinic system, both at HOMO and LUMO levels, feature consistent with the high degree of delocalization expected from such conjugated π system. The HOMO energy varies in the order **1 < 2 < 5 < 3 < 4** (**Table S11**), like the Ionization Potential (IP) values (**Table S1**) calculated for the hydroxylated derivatives **2-5**.

Thermochemical descriptors and antioxidant mechanisms

To give more insights about the preferred pathways used by **1-5** to exert their antioxidant properties, the three mechanisms commonly adopted by antioxidant phenolics were considered:[16,36,37] i) Hydrogen Atom Transfer (**HAT**); ii) Single Electron Transfer Proton Transfer (**SETPT**) and iii) Sequential Proton Loss Electron Transfer (**SPLET**). Results for all the studied compounds, computed for both gas phases and solvents (ethanol, water) are summarized in **Table S12**.

Calculated BDE values show that the introduction of a second -OH group in the 2-*H*-cromen-2-one backbone generally enhances the antioxidant activity of these molecules via HAT mechanism. The extent of this enhancement differs according to the position of the 2nd -OH group, being poorly influenced by the solvents used. For compounds **4** and **5**, having two -OH groups, there's a significative decrease in terms of BDE compared to their parent molecule **2**. In particular, the -OH group in the 7th position for **4** and the -OH group in the 8th position for **5** are those more prone to donate the H$^{\cdot}$. This trend is attributable to the catechol-like motif, present in both molecules, that promotes hydrogen transfer thanks to the H-bonds between the oxygen of the radicalized atom and the hydrogen of the neighbouring -OH group (**Fig. S20**). The same trend is also justified by the presence of a second -OH in ortho, thanks to its electro-releasing effect. As regards **3**, the BDEs are still lower, if compared to **2**, but not as much as **4** and **5**. This is due to the absence of the catecholic structure, but also because of the less significative electro-releasing effect of the 2nd -OH group

towards the 1st one (and vice versa), due to their relative substitution pattern in the 2-*H*-cromen-2-one moiety.

Calculated PAs show a trend similar to the one evidenced for BDEs, with the ligands **4** and **5** as the more inclined to release a proton (lower PA values), due to their catechol-like structure (**Fig. S21**).

It's interesting to notice how the PA values in a polar solvent are significantly lower than those in gas phase, suggesting a direct role of the solvent in the stabilization of the phenoxide anions, as reported for other compounds.[13,37] It's also curious to notice how the PA values in ethanol and water are significantly lower than the BDEs calculated in the same solvents. However, SPLET is a stepwise process, thus it is necessary to consider ETE values to determine the preferred antioxidant pathway. For this reason, the global descriptor SPLET, defined as the sum of PA and ETE values, was defined. By comparing the results obtained from SPLET descriptor with BDEs, we can observe how the BDEs are still lower than SPLETs. For this reason, SPLET mechanism can be ruled out as potential antioxidant mechanism for **2-5** in the gas phase, but also in polar medium like ethanol and water, even if becomes more competitive towards HAT.

IP and PDE values show that, for gas phase and ethanol, the IPs are considerably greater than PDEs, and vice versa in water. Thus, IP could be thought as the limiting step of SET-PT pathway in gas and ethanol, while in water the same key step is defined by PDE. Anyway, considering that also SET-PT is a stepwise process, the cumulative descriptor SET-PT, defined as the sum of IP and PDE values, was preferably considered. BDEs are still lower than the SET-PTs, although in polar medium the gap between these two descriptors became smaller.

In conclusion, HAT mechanism is confirmed as main pathway followed by **2-5** in gas phase and in the studied polar mediums. According to the BDEs, the antioxidant properties increases following the same order observed from experimental DPPH assay (**2 < 3 < 4 ≈ 5**).

Protonation sequencies

The protonation sequence and the structures of the different protonated species of **1**-**5** were evaluated by means of DFT calculations in water, using the same computational setup previously adopted. For

each calculated structure, the rotational barrier of the pyridine ring was evaluated through a Potential Energy Surface (PES) scan along the dihedral C7-C6-C5-N1 angle ($\tau = 0°$ and $\tau = 180°$ for the periplanar and antiperiplanar conformations, respectively), observing that distorted antiperiplanar conformations were generally adopted by all the species. However, the very modest energy required to switch to the lowest-energy distorted periplanar conformations, indicates that both the conformations are expected in solutions. The PES scans and structures of the lowest energy conformers are reported in **Fig. S22-S26**.

As regards the mono-cationic species $\mathbf{HL^+}$ for **1**, $\mathbf{H_2L^+}$ for **2**, $\mathbf{H_3L^+}$ for **3-5**, the lowest energy conformer (periplanar) is further stabilized by the pyridinic ring N–H···O intramolecular hydrogen bond (**Fig. S19**). This conformation was observed also in the crystal structure of $\mathbf{1{\cdot}HClO_4}$.[47] The species $\mathbf{H_2L}$ of **3** will lose the proton from the -OH group in the 5th position of its backbone, while **4** and **5** from the -OH group in the 7th and 8th position, respectively (see PA values in **Table 5**). By combining all the theoretical data with the experimental ones, the protonation sequencies reported in **Fig. S27-S31** have been proposed.

Molecular Docking

Molecular docking calculations were performed for **1-5** using the structure of Soybean Lipoxygenase-1 (PDB:3PZW) as receptor model. At pH 7.4, where the lipoxygenase inhibition was tested, **1** exists mainly in its neutral form, while **2-5** are mostly in their monoanionic form $\mathbf{L^-}$ for **2**, and $\mathbf{HL^-}$ for **3-5**. The highest-ranking score for the most potent molecule of the series **2** (in its mono-anionic form) is reported in **Fig. 5**, while for the other compounds are shown in **Fig. S32-S35**. All the studied ligands interact with the receptor in the same binding site, adopting different orientations and different kinds of non-covalent interactions with the surrounding residues, mainly π interactions (**Fig. 6**), according to the relative positions of the hydroxyl groups in the coumarinic backbone. These findings suggest a potential allosteric inhibitions mechanism adopted by the studied molecules that might take place in several ways:[68–71] for instance, by decreasing the binding affinity for the enzyme substrate or by

acting as scavengers towards the radical intermediates derived from linoleate peroxidation (especially for the hydroxylated derivatives).

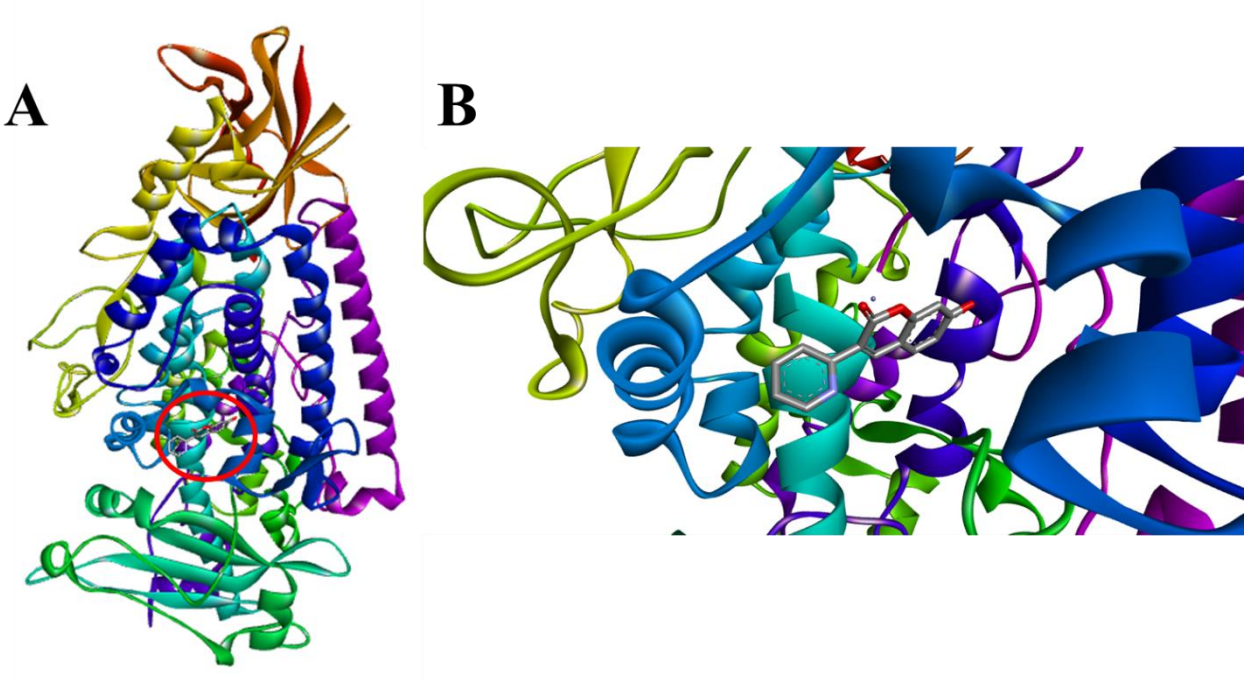

Fig. 5. Full view of the complex between the highest-ranking score of **2** (in its monoanionic form $\mathbf{L}^-$) and soybean lipoxygenase (**A**); zoom of the binding pocket occupied by the highest-ranking score of **2** (in its monoanionic form $\mathbf{L}^-$) and soybean lipoxygenase (**B**).

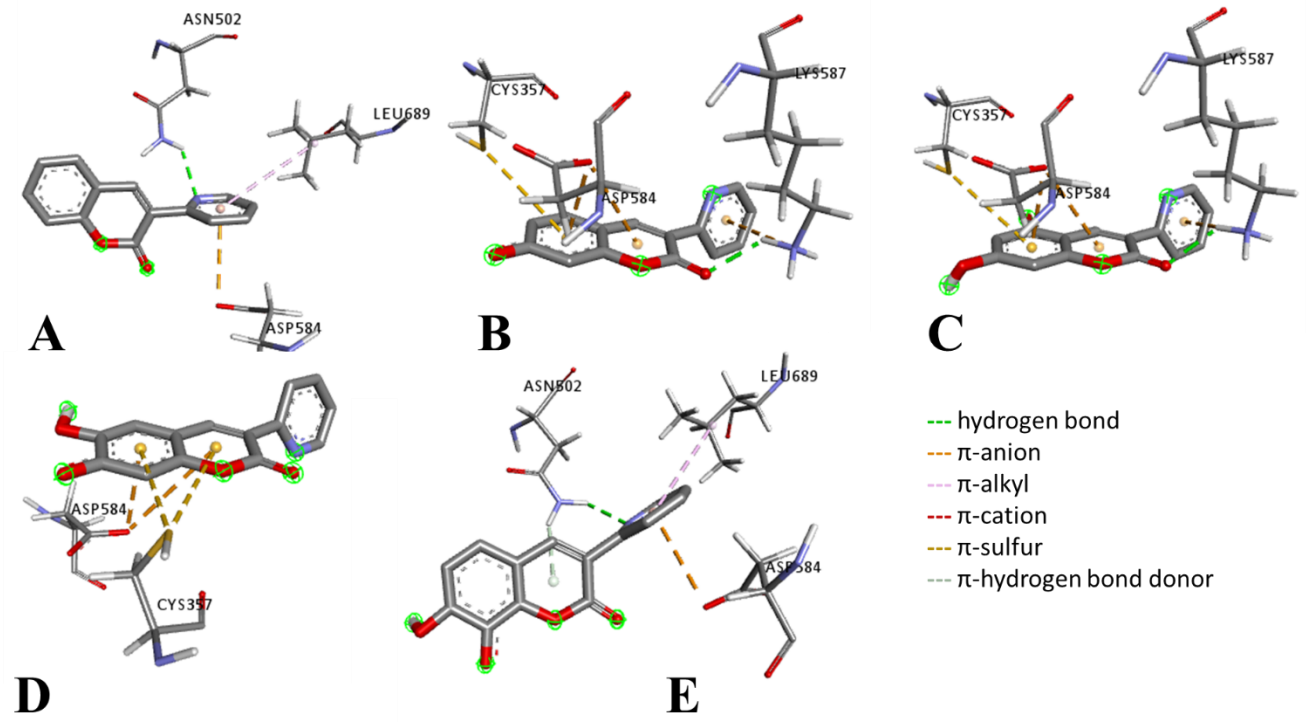

Fig. 6. Docked poses of **1** (**A**), **2** (as $\mathbf{L}^-$, **B**), **3** (as $\mathbf{HL}^-$, **C**), **4** (as $\mathbf{HL}^-$, **D**), **5** (as $\mathbf{HL}^-$, **E**) and intermolecular interactions with the surrounding residues of soybean lipoxygenase.

Conclusions

The study reported in this manuscript highlights how the insertion of the hydroxyl groups in the structure of 3-(pyridin-2-yl)coumarin increases the lipoxygenase inhibition and the antioxidant activities of these derivatives. Moreover, experimental results show how not only the insertion of a 2nd hydroxyl group, but also its position in the 3-(pyridin-2-yl)coumarin backbone play a key role in the definition of the biological properties of these molecules. A Hydrogen Atom Transfer mechanism was put in evidence as the preferred way to exert the antioxidant properties of the studied coumarins, whose potential absorption and bioavailability were preliminary evaluated by combining the experimental study of the protonation constants and the *in silico* evaluation of selected descriptors. All this, in term of results and approach, could be useful in the design and synthesis of novel compounds with potential biological properties.

Acknowledgments

S. M. acknowledges MIUR for his PhD fellowship (XXXIV cycle). We acknowledge the CeSAR (Centro Servizi Ricerca d'Ateneo) core facility of the University of Cagliari and Dr Sandrina Lampis for assistance with the generation of NMR data.

References

1 O. Kayser and H. Kolodziej, *Zeitschrift fur Naturforsch. - Sect. C J. Biosci.*, 1999, **54**, 169–174.

2 I. Kostova, S. Bhatia, P. Grigorov, S. Balkansky, V. S. Parmar, A. K. Prasad and L. Saso, *Curr. Med. Chem.*, 2011, **18**, 3929–3951.

3 G. Kirsch, A. Abdelwahab and P. Chaimbault, *Molecules*, 2016, **21**, 1322.

4 S. Emami and S. Dadashpour, *Eur. J. Med. Chem.*, 2015, **102**, 611–630.

5 L. He, T. He, S. Farrar, L. Ji, T. Liu and X. Ma, *Cell. Physiol. Biochem.*, 2017, **44**, 532–553.

6 R. L. Auten and J. M. Davis, *Pediatr. Res.*, 2009, **66**, 121–127.

7 A. R. Brash, *J. Biol. Chem.*, 1999, **274**, 23679–23682.

8 O. Rådmark, O. Werz, D. Steinhilber and B. Samuelsson, *Trends Biochem. Sci.*, 2007, **32**, 332–341.

9 D. A. Yanes and J. L. Mosser-Goldfarb, *J. Am. Acad. Dermatol.*, 2018, **78**, S71–S75.

10 F. Bruno, G. Spaziano, A. Liparulo, F. Roviezzo, S. M. Nabavi, A. Sureda, R. Filosa and B. D'Agostino, *Eur. J. Med. Chem.*, 2018, **153**, 65–72.

11 R. Wisastra and F. Dekker, *Cancers (Basel).*, 2014, **6**, 1500–1521.

12 G. Morabito, D. Trombetta, K. Singh Brajendra, K. Prasad Ashok, S. Parmar Virinder, C. Naccari, F. Mancari, A. Saija, M. Cristani and O. Firuzi, *Biochimie*, 2010, **92**, 1101–1107.

13 J. B. Veselinović, A. M. Veselinović, Ž. J. Vitnik, V. D. Vitnik and G. M. Nikolić, *Chem. Biol. Interact.*, 2014, **214**, 49–56.

14 T. C. Ngo, T. V. T. Mai, T. T. Pham, S. Jeremic, Z. Markovic, L. K. Huynh and D. Q. Dao, *Chem. Phys. Lett.*, 2020, **746**, 137312.

15 V. D. Kancheva, A. K. Slavova-Kazakova, S. E. Angelova, S. K. Singh, S. Malhotra, B. K. Singh, L. Saso, A. K. Prasad and V. S. Parmar, *Biochimie*, 2017, **140**, 133–145.

16 G. Mazzone, N. Malaj, A. Galano, N. Russo and M. Toscano, *RSC Adv.*, 2015, **5**, 565–575.

17 S. Vazquez-Rodriguez, R. Figueroa-Guíñez, M. J. Matos, L. Santana, E. Uriarte, M. Lapier, J. D. Maya and C. Olea-Azar, *Medchemcomm*, 2013, **4**, 993.

18 D. Sanna, V. Ugone, G. Micera, T. Pivetta, E. Valletta and E. Garribba, *Inorg. Chem.*, 2015, **54**, 8237–8250.

19 F. Gaccioli, R. Franchi-Gazzola, M. Lanfranchi, L. Marchiò, G. Metta, M. A. Pellinghelli, S. Tardito and M. Tegoni, *J. Inorg. Biochem.*, 2005, **99**, 1573–1584.

20 T. Pivetta, F. Trudu, E. Valletta, F. Isaia, C. Castellano, F. Demartin, R. Tuveri, S. Vascellari and A. Pani, *J. Inorg. Biochem.*, 2014, **141**, 103–113.

21 A. A. El-Sherif and T. M. A. Eldebss, *Spectrochim. Acta - Part A Mol. Biomol. Spectrosc.*, 2011, **79**, 1803–1814.

22 F. Sabuzi, S. Lentini, F. Sforza, S. Pezzola, S. Fratelli, O. Bortolini, B. Floris, V. Conte and P. Galloni, *J. Org. Chem.*, 2017, **82**, 10129–10138.

23 É. A. Enyedy, N. V. May, V. F. S. Pape, P. Heffeter, G. Szakács, B. K. Keppler and C. R. Kowol, *Dalt. Trans.*, 2020, **49**, 16887–16902.

24 A. Albert and E. P. Serjeant, *The Determination of Ionization Constants*, Springer Netherlands, Dordrecht, 1984.

25 P. Gans, *Talanta*, 2000, **51**, 33–37.

26 P. Gans, A. Sabatini and A. Vacca, *Talanta*, 1996, **43**, 1739–1753.

27 L. Alderighi, P. Gans, A. Ienco, D. Peters, A. Sabatini and A. Vacca, *Coord. Chem. Rev.*, 1999, **184**, 311–318.

28 E. Pontiki and D. Hadjipavlou-Litina, *Bioorganic Med. Chem.*, 2007, **15**, 5819–5827.

29 F. Neese, *Wiley Interdiscip. Rev. Comput. Mol. Sci.*, 2012, **2**, 73–78.

30 M. D. Hanwell, D. E. Curtis, D. C. Lonie, T. Vandermeersch, E. Zurek and G. R. Hutchison, *J. Cheminform.*, 2012, **4**, 17.

31 C. Adamo and V. Barone, *J. Chem. Phys.*, 1999, **110**, 6158–6170.

32 F. Weigend and R. Ahlrichs, *Phys. Chem. Chem. Phys.*, 2005, **7**, 3297.

33 V. Barone and M. Cossi, *J. Phys. Chem. A*, 1998, **102**, 1995–2001.

34 Chemcraft - graphical software for visualization of quantum chemistry computations. https://www.chemcraftprog.com.

35 T. Y. Nikolaienko, L. A. Bulavin and D. M. Hovorun, *Comput. Theor. Chem.*, 2014, **1050**, 15–22.

36 J. S. Wright, E. R. Johnson and G. A. DiLabio, *J. Am. Chem. Soc.*, 2001, **123**, 1173–1183.

37 L. Tabrizi, T. L. A. Nguyen and D. Q. Dao, *RSC Adv.*, 2019, **9**, 17220–17237.

38 C. Y. Lee, A. Sharma, J. Semenya, C. Anamoah, K. N. Chapman and V. Barone, *Antioxidants*, 2020, **9**, 189.

39 J. Kumar, N. Kumar, N. Sati and P. K. Hota, *New J. Chem.*, 2020, **44**, 8960–8970.

40 J. E. Bartmess, *J. Phys. Chem.*, 1994, **98**, 6420–6424.

41 Z. Marković, J. Tošović, D. Milenković and S. Marković, *Comput. Theor. Chem.*, 2016, **1077**, 11–17.

42 Molinspiration Cheminformatics free web services, https://www.molinspiration.com, Slovensky Grob, Slovakia.

43 O. Trott and A. J. Olson, *J. Comput. Chem.*, 2009, 455–461.

44 G. M. Morris, H. Ruth, W. Lindstrom, M. F. Sanner, R. K. Belew, D. S. Goodsell and A. J. Olson, *J. Comput. Chem.*, 2009, **30**, 2785–2791.

45 Dassault Systèmes BIOVIA, Discovery Studio Viewer, v19, San Diego: Dassault Systèmes, 2019.

46 T. Pivetta, S. Masuri, M. G. Cabiddu, C. Caltagirone, A. Pintus, M. Massa, F. Isaia and E.

Cadoni, *New J. Chem.*, 2019, **43**, 12032–12041.

47 T. Pivetta, E. Valletta, G. Ferino, F. Isaia, A. Pani, S. Vascellari, C. Castellano, F. Demartin, M. G. Cabiddu and E. Cadoni, *J. Inorg. Biochem.*, 2017, **177**, 101–109.

48 O. V Khilya, O. V Shablykina, M. S. Frasinyuk, V. V Ishchenko and V. P. Khilya, *Chem. Nat. Compd.*, 2005, **41**, 523–528.

49 K. Yoshiyuki, O. Hiromichi, A. Shigeru, B. Kimiye and K. Mitsugi, *Biochim. Biophys. Acta (BBA)/Lipids Lipid Metab.*, 1985, **834**, 224–229.

50 G. Kanimozhi, N. R. Prasad, S. Ramachandran and K. V. Pugalendi, *Eur. J. Pharmacol.*, 2011, **672**, 20–29.

51 A. Witaicenis, L. N. Seito, A. Da Silveira Chagas, L. D. De Almeida, A. C. Luchini, P. Rodrigues-Orsi, S. H. Cestari and L. C. Di Stasi, *Phytomedicine*, 2014, **21**, 240–246.

52 N. Tomohiro, K. Yasuko and M. Sei-Itsu, *Biochim. Biophys. Acta (BBA)/Lipids Lipid Metab.*, 1983, **753**, 130–132.

53 B. N. Mattoo, *Trans. Faraday Soc.*, 1957, **53**, 760.

54 C. A. Lipinski, F. Lombardo, B. W. Dominy and P. J. Feeney, *Adv. Drug Deliv. Rev.*, 2001, **46**, 3–26.

55 P. Ertl, B. Rohde and P. Selzer, *J. Med. Chem.*, 2000, **43**, 3714–3717.

56 H. Pajouhesh and G. R. Lenz, *NeuroRx*, 2005, **2**, 541–553.

57 C. Fattuoni, S. Vascellari and T. Pivetta, *Amino Acids*, 2020, **52**, 397–407.

58 R. Zhou, P. Moench, C. Heran, X. Lu, N. Mathias, T. N. Faria, D. A. Wall, M. A. Hussain, R. L. Smith and D. Sun, *Pharm. Res.*, 2005, **22**, 188–192.

59 J. B. Dressman, G. L. Amidon, C. Reppas and V. P. Shah, *Pharm. Res.*, 1998, **15**, 11–22.

60 A. Phaniendra, D. B. Jestadi and L. Periyasamy, *Indian J. Clin. Biochem.*, 2015, **30**, 11–26.

61 M. Kataoka, K. Tonooka, T. Ando, K. Imai and T. Aimoto, *Free Radic. Res.*, 1997, **27**, 419–427.

62 M. Asanuma, S. Nishibayashi-Asanuma, I. Miyazaki, M. Kohno and N. Ogawa, *J.*

Neurochem., 2001, **76**, 1895–1904.

63 J. Z. Pedersen, C. Oliveira, S. Incerpi, V. Kumar, A. M. Fiore, P. De Vito, A. K. Prasad, S. V. Malhotra, V. S. Parmar and L. Saso, *J. Pharm. Pharmacol.*, 2007, **59**, 1721–1728.

64 D. Hadjipavlou-Litina, T. Garnelis, C. M. Athanassopoulos and D. Papaioannou, *J. Enzyme Inhib. Med. Chem.*, 2009, **24**, 1188–1193.

65 M. Roussaki, K. Zelianaios, E. Kavetsou, S. Hamilakis, D. Hadjipavlou-Litina, C. Kontogiorgis, T. Liargkova and A. Detsi, *Bioorganic Med. Chem.*, 2014, **22**, 6586–6594.

66 S. Masuri, E. Cadoni, M. G. Cabiddu, F. Isaia, M. G. Demuru, L. Moráň, D. Buček, P. Vaňhara, J. Havel and T. Pivetta, *Metallomics*, 2020, **12**, 891–901.

67 Y.-X. Da and Z.-J. Quan, *Acta Crystallogr. Sect. E Struct. Reports Online*, 2010, **66**, o2872–o2872.

68 V. Sanda and M. Jisak, in *Recent Trends for Enhancing the Diversity and Quality of Soybean Products*, InTech, 2011.

69 E. T. Denisov and I. B. Afanas'ev, *Oxidation and Antioxidants in Organic Chemistry and Biology*, CRC Press, 2005, vol. 128.

70 O. Kouzi, E. Pontiki and D. Hadjipavlou-Litina, *Molecules*, 2019, **24**, 1–20.

71 I. Kostopoulou, A. Diassakou, E. Kavetsou, E. Kritsi, P. Zoumpoulakis, E. Pontiki, D. Hadjipavlou-Litina and A. Detsi, *Mol. Divers.*, , DOI:10.1007/s11030-020-10045-x.